Probing Cold Dense Nuclear Matter

R. Subedi,[1] R. Shneor,[2] P. Monaghan,[3] B. D. Anderson,[1] K. Aniol,[4] J. Annand,[5] J. Arrington,[6]
H. Benaoum,[7,8] F. Benmokhtar,[9] W. Bertozzi,[3] W. Boeglin,[10] J.-P. Chen,[11] Seonho Choi,[12]
E. Cisbani,[13] B. Craver,[14] S. Frullani,[13] F. Garibaldi,[13] S. Gilad,[3] R. Gilman,[11,15]
O. Glamazdin,[16] J.-O. Hansen,[11] D. W. Higinbotham,[11*] T. Holmstrom,[17] H. Ibrahim,[18]
R. Igarashi,[19] C.W. de Jager,[11] E. Jans,[20] X. Jiang,[15] L.J. Kaufman,[9,22] A. Kelleher,[17]
A. Kolarkar,[23] G. Kumbartzki,[15] J. J. LeRose,[11] R. Lindgren,[14] N. Liyanage,[14]
D. J. Margaziotis,[4] P. Markowitz,[10] S. Marrone,[24] M. Mazouz,[25] D. Meekins,[11] R. Michaels,[11]
B. Moffit,[17] C. F. Perdrisat,[17] E. Piasetzky,[2] M. Potokar,[26] V. Punjabi,[27] Y. Qiang,[3]
J. Reinhold,[10] G. Ron,[2] G. Rosner,[28] A. Saha,[11] B. Sawatzky,[14,29] A. Shahinyan,[30] S. Širca,[26,31]
K. Slifer,[14] P. Solvignon,[29] V. Sulkosky,[17] G. M. Urciuoli,[13] E. Voutier,[25] J. W. Watson,[1]
L.B. Weinstein,[18] B. Wojtsekhowski,[11] S. Wood,[11] X.-C. Zheng,[3,6,14] and L. Zhu[32]

[1]Kent State University, Kent State, OH 44242, USA
[2]Tel Aviv University, Tel Aviv 69978, Israel
[3]Massachusetts Institute of Technology, Cambridge, MA 02139, USA
[4]California State University Los Angeles, Los Angeles, CA 90032, USA
[5]University of Glasgow, Glasgow G12 8QQ, Scotland, UK
[6]Argonne National Laboratory, Argonne, IL 60439, USA
[7]Syracuse University, Syracuse, NY 13244, USA
[8]Prince Mohammad University, Al-Khobar 31952, Saudi Arabia
[9]University of Maryland, College Park. MD 20742, USA
[10]Florida International University, Miami, FL 33199, USA
[11]Thomas Jefferson National Accelerator Facility, Newport News, VA 23606, USA
[12]Seoul National University, Seoul 151-747, Korea
[13]INFN, Sezione di Roma, I-00185 Rome, Italy
[14]University of Virginia, Charlottesville, VA 22904, USA
[15]Rutgers, The State University of New Jersey, Piscataway, NJ 08855, USA
[16]Kharkov Institute of Physics and Technology, Kharkov 310108, Ukraine
[17]College of William and Mary, Williamsburg, VA 23187, USA
[18]Old Dominion University, Norfolk, VA 23508, USA
[19]University of Saskatchewan, Saskatoon, Saskatchewan, Canada S7N 5E2
[20]Nationaal Instituut voor Subatomaire Fysica, Amsterdam, The Netherlands
[22]University of Massachusetts Amherst, Amherst, MA 01003, USA
[23]University of Kentucky, Lexington, KY 40506, USA
[24]Dipartimento di Fisica and INFN sez. Bari, Bari, Italy
[25]Laboratoire de Physique Subatomique et de Cosmologie, 38026 Grenoble, France
[26]Institute "Jožef Stefan", 1000 Ljubljana, Slovenia
[27]Norfolk State University, Norfolk, VA 23504, USA
[28]University of Glasgow, Glasgow G12 8QQ, Scotland, UK
[29]Temple University, Philadelphia, PA 19122, USA
[30]Yerevan Physics Institute, Yerevan 375036, Armenia
[31]Dept. of Physics, University of Ljubljana, 1000 Ljubljana, Slovenia
[32]University of Illinois at Urbana-Champaign, Urbana, IL 61801, USA

*To whom correspondence should be addressed; E-mail: doug@jlab.org.

1

The protons and neutrons in a nucleus can form strongly correlated nucleon pairs. Scattering experiments, where a proton is knocked-out of the nucleus with high momentum transfer and high missing momentum, show that in ^{12}C the neutron-proton pairs are nearly twenty times as prevalent as proton-proton pairs and, by inference, neutron-neutron pairs. This difference between the types of pairs is due to the nature of the strong force and has implications for understanding cold dense nuclear systems such as neutron stars.

Introduction

Nuclei are composed of bound protons and neutrons, referred to collectively as nucleons (the standard notation is p, n, and N, respectively). A standard model of the nucleus since the 1950s has been the nuclear shell model, where neutrons and protons move independently in well-defined quantum orbits in the average nuclear field created by their mutual attractive interactions. In the 1980s and 1990s, proton removal experiments using electron beams with energies of several hundred MeV showed that only 60-70% of the protons participate in this type of independent-particle motion in nuclear valence states (*1, 2*). At the time, it was assumed that this low occupancy was caused by correlated pairs of nucleons within the nucleus. Indeed, the existence of nucleon pairs that are correlated at distances of several femtometers, known as long-range correlations, has been established (*3*), but these accounted for less than half of the predicted correlated nucleon pairs. Recent high momentum transfer measurements (*4, 5, 6, 7, 8, 9, 10, 11, 12*) have shown that nucleons in nuclear ground states can form pairs with large relative momentum and small center-of-mass (CM) momentum due to the short-range, scalar and tensor, components of the nucleon-nucleon interaction. These pairs are referred to as short-range correlated (SRC) pairs. The study of these SRC pairs allows access to cold dense nuclear matter, such as that found in a neutron star.

Experimentally, a high-momentum probe can knock a proton out of a nucleus, leaving the rest of the system nearly unaffected. If, on the other hand, the proton being struck is part of a SRC pair, the high relative momentum in the pair would cause the correlated nucleon to recoil and be ejected as well (Fig. 1). High-momentum knock-out by both high-energy protons (*8, 9, 10*) and high-energy electrons (*12*) has shown, for kinematics far from particle production resonances, that when a proton with high missing momentum is removed from the ^{12}C nucleus, the momentum is predominantly balanced by a single recoiling nucleon. This is consistent with the theoretical description that large nucleon momenta in the nucleus are predominantly caused by SRC pairing (*13*). This effect has also been shown using inclusive (e,e') data (*4, 5, 14*), though that type of measurement is not sensitive to the type of SRC pair. Here, we identify the relative abundance of p-n and p-p SRC pairs in ^{12}C nuclei.

Equipment

We performed our experiment in Hall A of the Thomas Jefferson National Accelerator Facility (JLab) using an incident electron beam of 4.627 GeV with a beam current between 5 and 40 μA.

The beam was incident on a 0.25 mm thick pure ^{12}C sheet rotated 70° to the beam line to minimize the material through which the recoiling protons passed. We used the two Hall A high-resolution spectrometers (HRS) (*15*) to define proton-knockout events, ^{12}C(e,e'p). The left HRS detected scattered electrons at a central scattering angle (momentum) of 19.5° (3.724 GeV/c). These values correspond to the quasi-free knockout of a single proton with transferred three-momentum q = 1.65 GeV/c, transferred energy $\omega = 0.865$ GeV, $Q^2 = q^2 - (\omega/c)^2 = 2$ (GeV/c)^2, and Bjorken scaling parameter $x_B = Q^2/2m\omega = 1.2$, where m is the mass of the proton. The right HRS detected knocked-out protons at three different values for the central angle (momentum): 40.1° (1.45 GeV/c), 35.8° (1.42 GeV/c), and 32.0° (1.36 GeV/c). These kinematic settings covered (e,e'p) missing momenta, which is the momentum of the undetected particles, in the range of 300-600 MeV/c with overlap between the different settings. For highly correlated pairs, the missing momentum of the (e,e'p) reaction is balanced almost entirely by a single recoiling nucleon; whereas for a typical uncorrelated (e,e'p) event, the missing momentum is balanced by the sum of many recoiling nucleons. In a partonic picture, x_B is the fraction of the nucleon momentum carried by the struck quark. Hence, when $x_B > 1$, the struck quark has more momentum than the entire nucleon, which points to nucleon correlation. To detect correlated recoiling protons, a large acceptance spectrometer (BigBite) was placed at an angle of 99° w.r.t. the beam direction and 1.1 m from the target. To detect correlated recoiling neutrons, a neutron array was placed directly behind the BigBite spectrometer at a distance of 6 m from the target. Details of these custom proton and neutron detectors can be found in the supporting on-line materials.

Analysis and Results

The electronics for the experiment were set up such that for every ^{12}C(e,e'p) event in the HRS spectrometers, we read out the BigBite and the neutron-detector electronics; thus, we could determine the ^{12}C(e,e'pp)/^{12}C(e,e'p) and the ^{12}C(e,e'pn)/^{12}C(e,e'p) ratios. For the ratio ^{12}C(e,e'pp)/^{12}C(e,e'p), we found that 9.5 ± 2% of the (e,e'p) events had an associated recoiling proton as reported in (*12*). Taking into account the finite acceptance of the neutron detector, using the same procedure as was done for the proton detector (*12*), and the neutron detection efficency, we found that 96 ± 22% of the (e,e'p) events with a missing momentum above 300 MeV/c had a recoiling neutron. This result agrees with a hadron beam measurement of (p,2pn)/(p,2p) in which 92 ± 18% of the (p,2p) events with a missing momentum above the Fermi momentum of 275 MeV/c were found to have a single recoiling neutron carrying the momentum (*11*).

Since we collected the recoiling proton ^{12}C(e,e'pp) and neutron ^{12}C(e,e'pn) data simultaneously with detection systems covering nearly identical solid angles, we could also directly determine the ratio of ^{12}C(e,e'pn)/^{12}C(e,e'pp). In this scheme, many of the systematic factors needed to compare the rates of the ^{12}C(e,e'pn) and ^{12}C(e,e'pp) reactions canceled out. Correcting only for detector efficiencies, we determined that this ratio was 8.1±2.2. To estimate the effect of final-state interactions (i.e., reactions that happen after the initial scattering), we assumed that the attenuation of the recoiling protons and neutrons were almost equal. In this case,

the only correction related to final-state interactions of the measured ^{12}C(e,e'pn) to ^{12}C(e,e'pp) ratio is due to single charge exchange. Since the measured (e,e'pn) rate is about an order of magnitude larger than the (e,e'pp) rate, (e,e'pn) reactions followed by single charge exchange (and hence detected as (e,e'pp)) dominate and reduced the measured ^{12}C(e,e'pn)/^{12}C(e,e'pp) ratio. Using the Glauber approximation (*16*), we estimated this effect was 11%. Taking this into account, the corrected experimental ratio for ^{12}C(e,e'pn)/^{12}C(e,e'pp) is 9.0±2.5.

To deduce the ratio of p-n to p-p SRC pairs in the ground state of ^{12}C, we use the measured ^{12}C(e,e'pn) to ^{12}C(e,e'pp) ratio. Because we used (e,e'p) events to search for SRC nucleon pairs, the probability of detecting p-p pairs was twice that of p-n pairs; thus, we conclude that the ratio of p-n/p-p pairs in the ^{12}C ground state is 18±5 as shown in Fig. 2. To get a comprehensive picture of the structure of ^{12}C, we combined the pair faction results with the inclusive ^{12}C(e,e') measurements (*4,5,14*) where it was found that approximately 20% of the nucleons in ^{12}C form SRC pairs: a result consistent with the the depletion seen in the spectroscopy experiments (*1,2*). As shown in Fig. 3, the combined results indicate 80% of the nucleons in the ^{12}C nucleus acted independent or as described within the shell model, whereas for the 20% of correlated pairs, 90±10% were in the form of p-n SRC pairs, 5±1.5% were in the form of p-p SRC pairs, and by isospin symmetry infer that 5±1.5% were in the form of SRC n-n pairs. The dominance of the p-n over p-p SRC pairs is a clear consequence of the nucleon-nucleon tensor force. Calculations of this effect (*17,18*) indicate that it is robust and does not depend on the exact parameterization of the nucleon-nucleon force, the type of the nucleus, or the exact ground-state wave-function used to describe the nucleons.

If neutron stars consisted of neutrons only, the relatively weak n-n short-range interaction would mean that they could be reasonably well approximated as an ideal Fermi gas, with only perturbative corrections. However, theoretical analysis of neutrino cooling data indicates that neutron stars contain about 5-10% protons and electrons in the first central layers (*19,20,21*). The strong p-n short-range interaction reported here suggests that momentum distribution for the protons and for the neutrons in neutron stars will be substantially different from that characteristic of an ideal Fermi gas. A theoretical calculation that takes into account the p-n correlation effect at relevant neutron star densities and realistic proton concentration shows the correlation effect on the momentum distribution of the protons and the neutrons (*22*). We therefore speculate that the small concentration of protons inside neutron stars might have a disproportionately large effect that needs to be addressed in realistic descriptions of neutron stars.
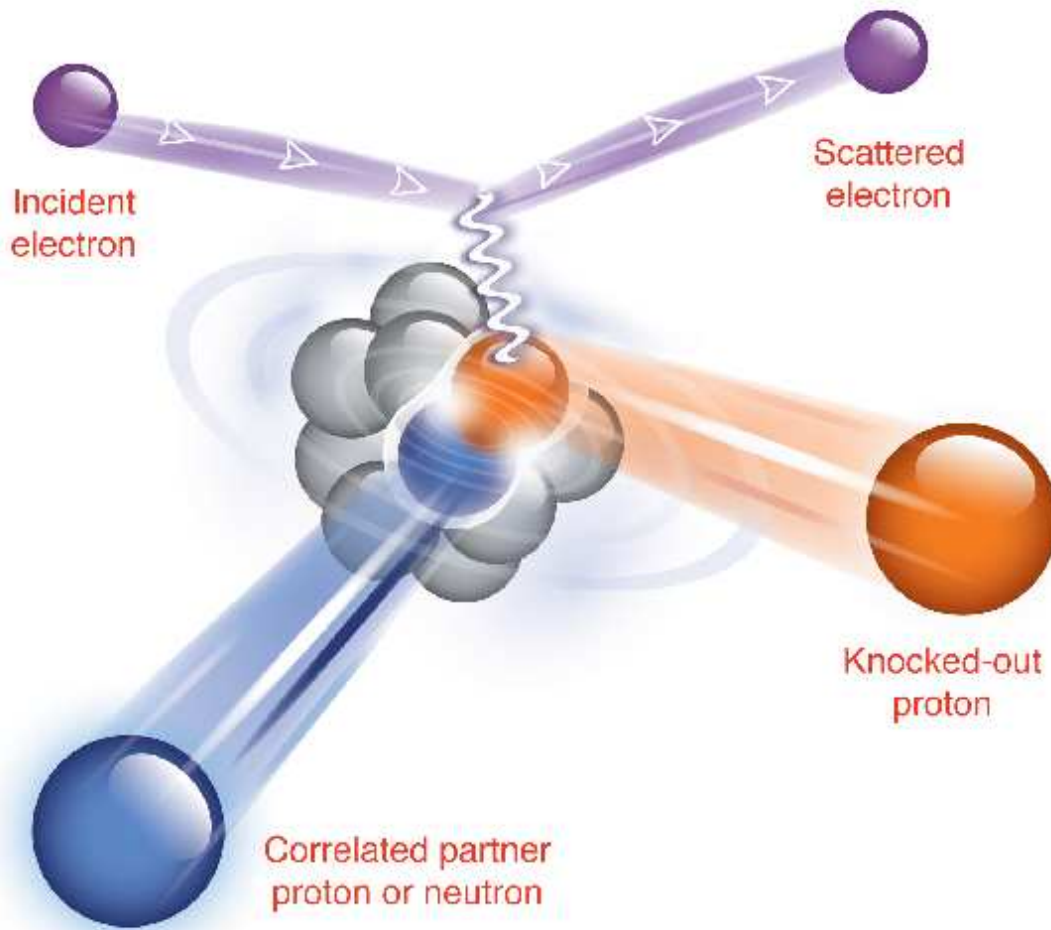
Figure 1: Illustration of the ^{12}C(e,e'pN) reaction. The incident electron beam couples to a nucleon-nucleon pair via a virtual photon. In the final state, the scattered electron is detected along with the two nucleons that are ejected from the nucleus. Typical nuclear density is about 0.16 nucleons/fm^3 while for pairs the local density is approximately 5 times larger.
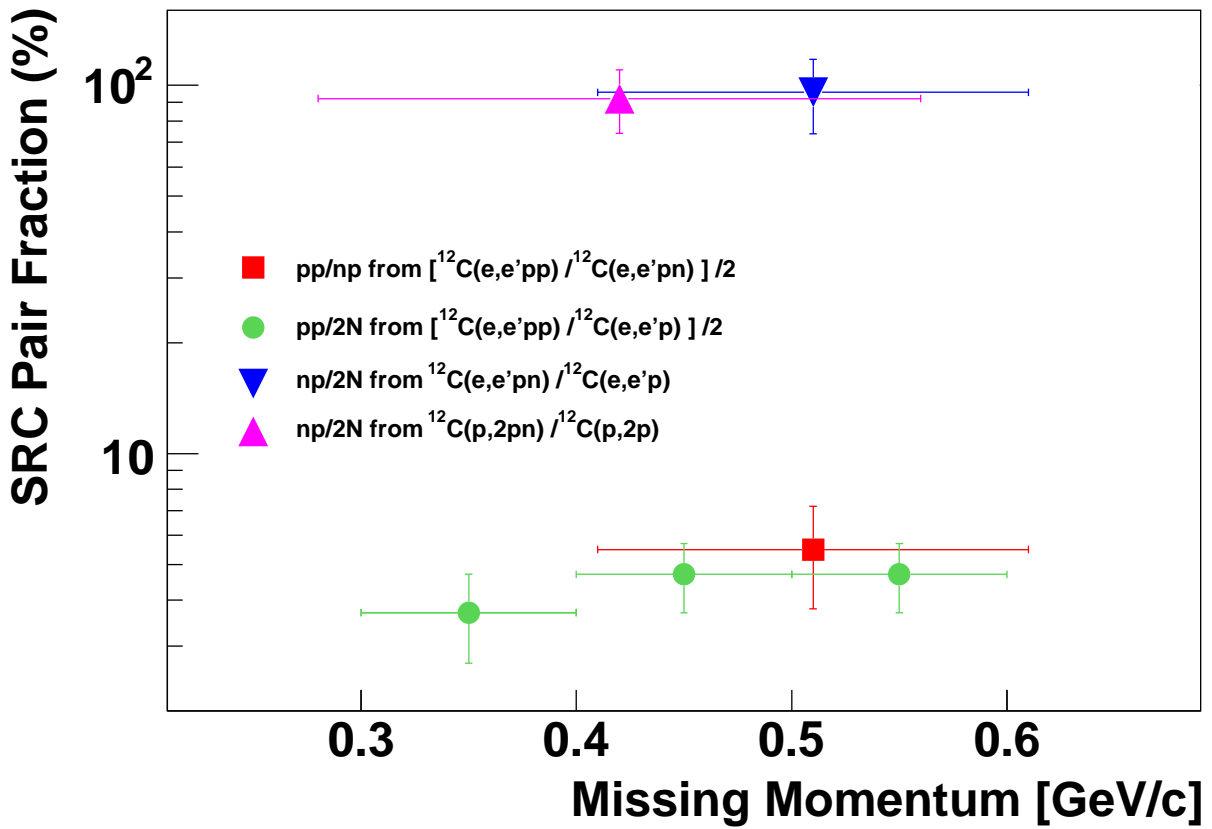
Figure 2: The fractions of correlated pair combinations in carbon as obtained from the (e,e'pp) and (e,e'pn) reactions, as well as from previous (p,2pn) data. The results and references are listed in Table 1.
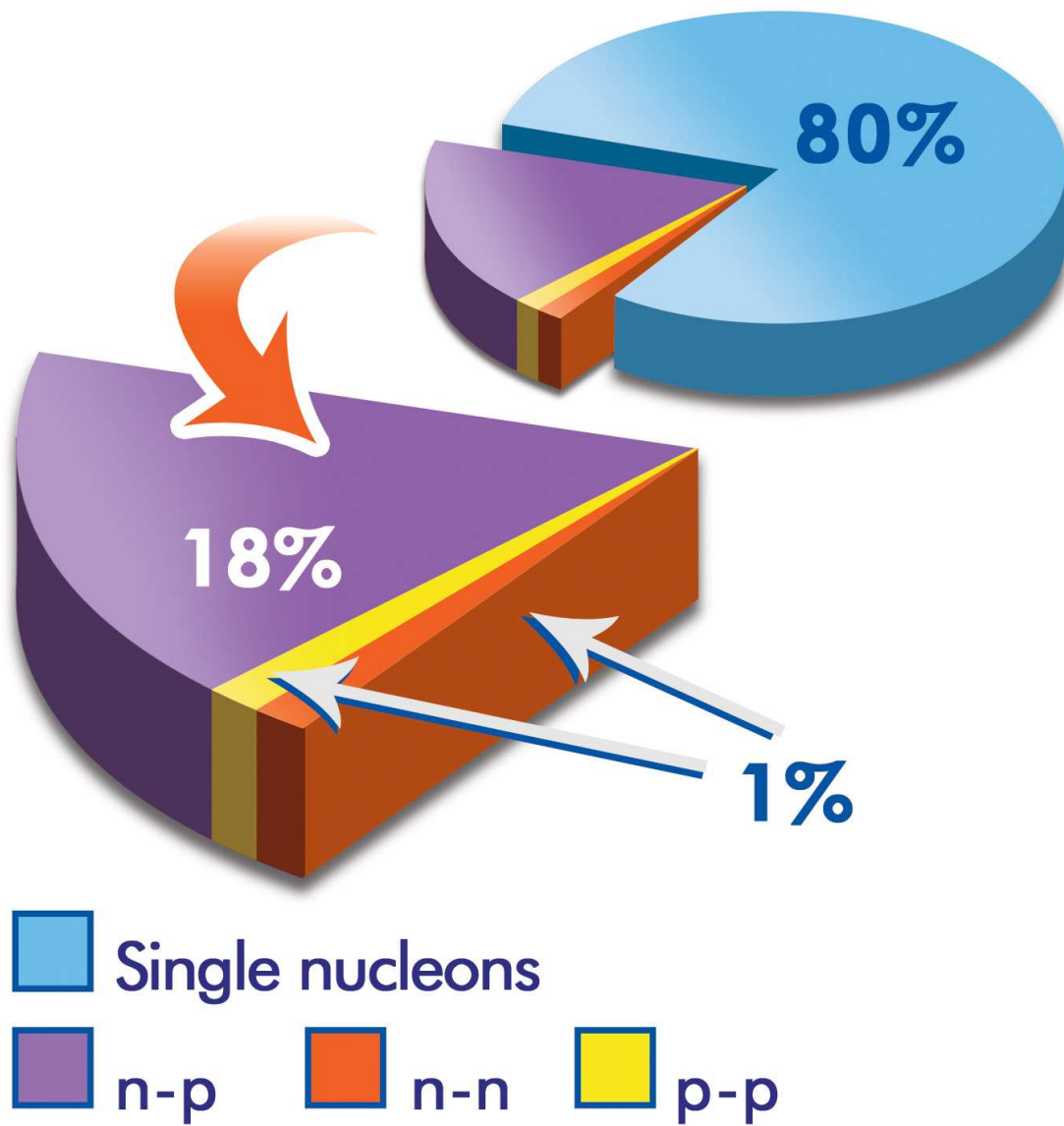
Figure 3: The average fraction of nucleons in the various initial state configurations of ^{12}C.

Supporting Materials

The experiment was performed in Hall A of the Continuous Electron Beam Accelerator Facility (CEBAF) located at the Thomas Jefferson National Accelerator Facility in Newport News, VA (*23*). Along with the standard Hall A equipment (*15*), the experiment required a new proton spectrometer and neutron detector as well as a new scattering chamber to accommodate the large out-of-plane acceptance of these detectors (see Fig. 4).
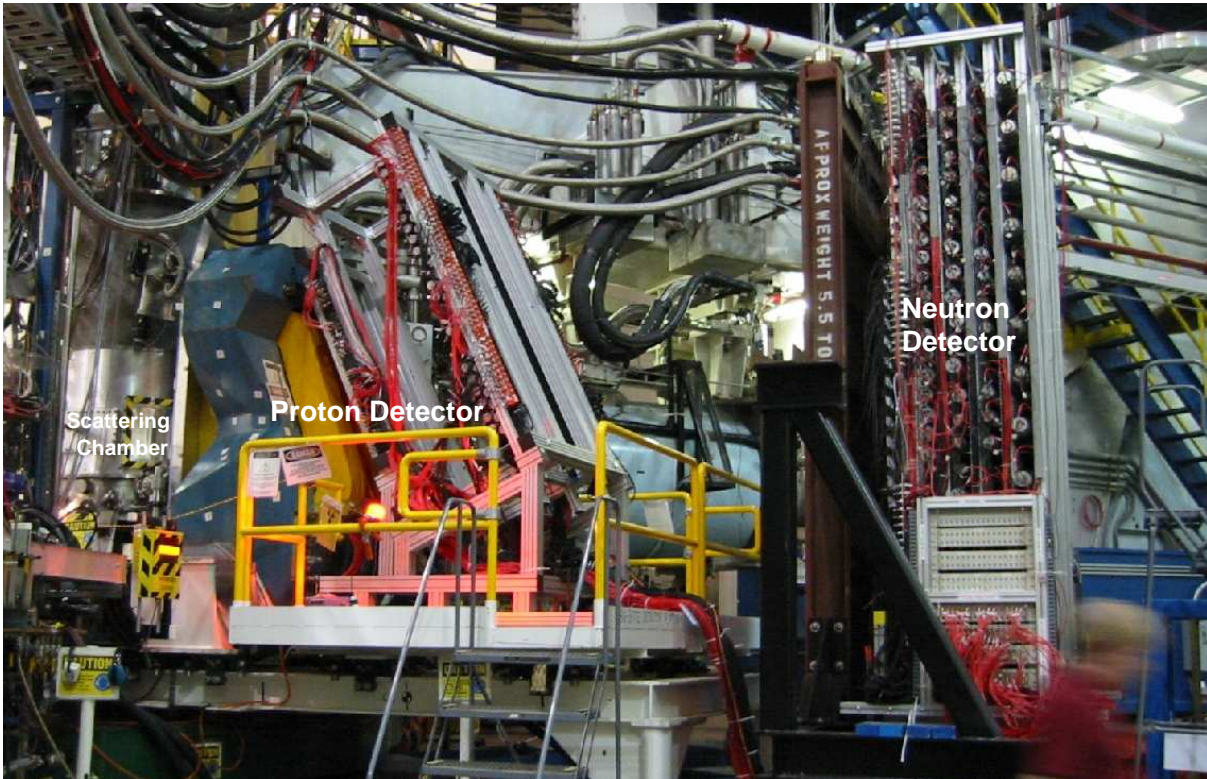

Figure 4: Photograph of the proton and neutron detectors in experimental Hall A.

Proton Spectrometer

The proton spectrometer (BigBite) consists of a large-acceptance, non-focusing dipole magnet and a customized detector package. For this experiment, the spectrometer was at an angle of $99°$ w.r.t. the beam direction and 1.1 m from the target with a resulting angular acceptance of about 96 msr and a nominal momentum acceptance from 0.25 GeV/c to 0.9 GeV/c. The detector package consisted of three planes of plastic scintillator segmented in the dispersive direction. This unshielded system was able to run in Hall A with a luminosity of up to 10^{38} cm^{-2}s^{-1}.

The non-focusing magnetic dipole, with a central field of 0.93 T, was used to bend the charged particles before they hit the detector planes. Timing, hit position, and energy deposited in the scintillators were all used to determine the incoming particle direction and momentum.

The detector achieved an angular resolution of 1.5 mrad in both the vertical and horizontal planes. The timing resolution of the trigger plane scintillators was measured to be 0.5 nsec. This timing resolution along with path length correction translated to a momentum resolution of $\delta p/p = 2.5\%$.

Neutron Detector

To detect recoiling neutrons, 88 plastic scintillator bars were placed directly behind the BigBite spectrometer at a distance of 6 m from the target. The detector had a width of 1 m, a height of 3 m, and a depth of 0.4 m. A 5 cm thick lead wall was placed in front of the detector to block low-energy photons and most of the charged particles while allowing most neutrons to pass. A layer of 2 cm thick plastic scintillators was placed between the lead wall and the neutron detector to identify any charged particles that managed to pass through the lead wall. The detector covered a solid angle similar to that of BigBite.

The absolute probability for the detector to detect a neutron that originated at the target was determined using the ^{2}H(e,e'p)n reaction and checking the result against a simulation code that takes into account the attenuation of the neutron flux and the neutron detection efficiency of the plastic scintillators (*24*). The results of this calibration are shown in Fig. 5.

Reaction	Missing Momentum [MeV]	Pair Fraction	Mean±SD [%]	Reference
[^{12}C(e,e'pp)/^{12}C(e,e'pn)]/2	0.41 - 0.51	pp/pn	5.5 ± 1.5	This Work
[^{12}C(e,e'pp)/^{12}C(e,e'p)]/2	0.30 - 0.40	pp/2N	3.7 ± 1	(*12*)
[^{12}C(e,e'pp)/^{12}C(e,e'p)]/2	0.40 - 0.50	pp/2N	4.7 ± 1	(*12*)
[^{12}C(e,e'pp)/^{12}C(e,e'p)]/2	0.50 - 0.60	pp/2N	4.7 ± 1	(*12*)
^{12}C(e,e'pn)/^{12}C(e,e'p)	0.41 - 0.61	pn/2N	96 ± 22	This Work
^{12}C(p,ppn)/^{12}C(p,pp)	0.28 - 0.56	pn/2N	92 ± 18	(*11*)

Table 1: Table of nucleon-nucleon pair fraction extracted along with the statistical error. In the systematical error, the dominant contribution is the correlated uncertainty of approximately 10% of the mean for the ^{12}C(e,e'pn)/^{12}C(e,e'p) and ^{12}C(e,e'pp)/^{12}C(e,e'p) results due to an acceptance correction which is limited by the knowledge of pair motion in the nucleus (*12*). For the ratio of ^{12}C(e,e'pp)/^{12}C(e,e'pn) this systematic effect cancels.
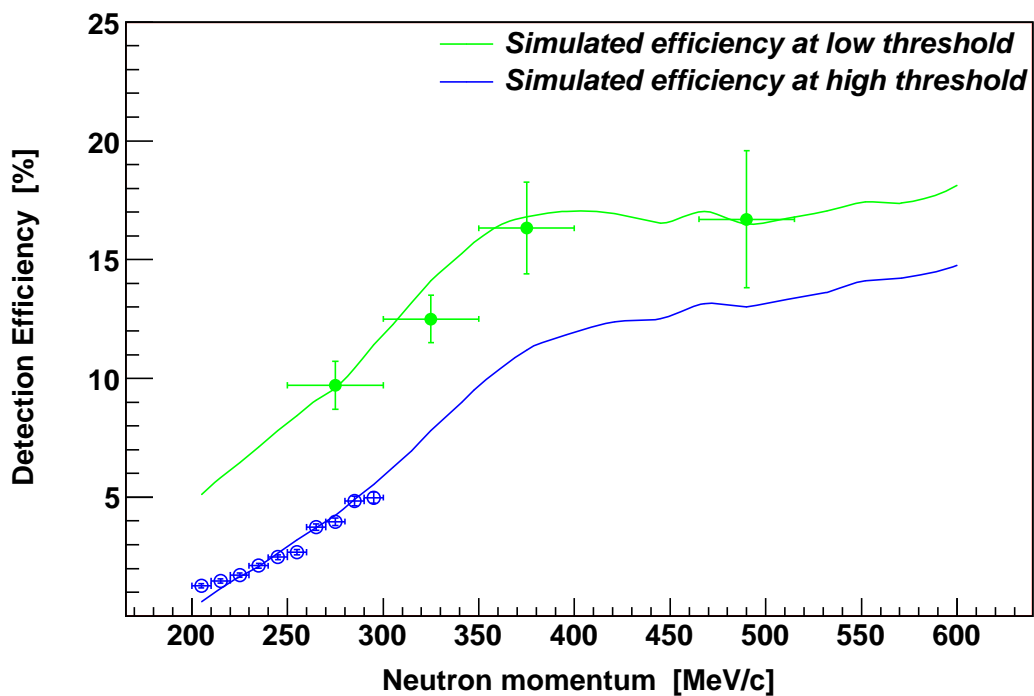
Figure 5: Shown is the neutron detection efficiency versus neutron momentum. The data are from the overdetermined quasi-elastic $^2\mathrm{H}(e, e'p)n$ reaction, which was used to make an effective neutron beam while the curves are from a simulation. The green curve is for a 4.627 GeV beam and a low detection threshold, while the blue curve is for a 2.345 GeV beam with a high detection threshold.

References and Notes

1. L. Lapikas, *Nucl. Phys.* **A553**, 297 (1993).

2. J. Kelly, *Adv. Nucl. Phys.* **23**, 75 (1996).

3. W. H. Dickhoff, C. Barbieri, *Prog. Part. Nucl. Phys.* **52**, 377 (2004).

4. K. S. Egiyan, *et al.*, *Phys. Rev.* **C68**, 014313 (2003).

5. K. S. Egiyan, *et al.*, *Phys. Rev. Lett.* **96**, 082501 (2006).

6. R. A. Niyazov, *et al.*, *Phys. Rev. Lett.* **92**, 052303 (2004).

7. F. Benmokhtar, *et al.*, *Phys. Rev. Lett.* **94**, 082305 (2005).

8. J. L. S. Aclander, *et al.*, *Phys. Lett.* **B453**, 211 (1999).

9. A. Tang, *et al.*, *Phys. Rev. Lett.* **90**, 042301 (2003).

10. A. Malki, *et al.*, *Phys. Rev.* **C65**, 015207 (2002).

11. E. Piasetzky, M. Sargsian, L. Frankfurt, M. Strikman, J. W. Watson, *Phys. Rev. Lett.* **97**, 162504 (2006).

12. R. Shneor, *et al.*, *Phys. Rev. Lett.* **99**, 072501 (2007).

13. L. L. Frankfurt, M. I. Strikman, *Phys. Rept.* **76**, 215 (1981).

14. L. L. Frankfurt, M. I. Strikman, D. B. Day, M. Sargsian, *Phys. Rev.* **C48**, 2451 (1993).

15. J. Alcorn, *et al.*, *Nucl. Instrum. Meth.* **A522**, 294 (2004).

16. I. Mardor, Y. Mardor, E. Piasetzky, J. Alster, M. M. Sargsian, *Phys. Rev.* **C46**, 761 (1992).

17. R. Schiavilla, R. B. Wiringa, S. C. Pieper, J. Carlson, *Phys. Rev. Lett.* **98**, 132501 (2007).

18. M. M. Sargsian, T. V. Abrahamyan, M. I. Strikman, L. L. Frankfurt, *Phys. Rev.* **C71**, 044615 (2005).

19. J. M. Lattimer, M. Prakash, *Science* **304**, 536 (2004).

20. G. Baym, *Nucl. Phys.* **A590**, 233 (1995).

21. G. Baym, *Nucl. Phys.* **A702**, 3 (2002).

22. T. Frick, H. Muther, A. Rios, A. Polls, A. Ramos, *Phys. Rev.* **C71**, 014313 (2005).

23. C. W. Leeman, D. R. Douglas, G. A. Krafft, *Annu. Rev. Nucl. Part. Sci.* **51**, 413 (2001).

24. R. A. Cecil, B. D. Anderson, R. Madey, *Nucl. Instrum. Meth.* **161**, 439 (1979).

25. This work was supported by the Israel Science Foundation, the US-Israeli Bi-national Scientific Foundation, the UK Engineering and Physical Sciences Research Council and the Science & Technology Facilities Council, the U.S. National Science Foundation, the U.S. Department of Energy grants DE-AC02-06CH11357, DE-FG02-94ER40818, and U.S. DOE Contract No. DE-AC05-84150, Modification No. M175, under which the Southeastern Universities Research Association, Inc. operates the Thomas Jefferson National Accelerator Facility. The raw data from this experiment is archived in Jefferson Lab's mass storage silo in the directory /mss/halla/e01015/raw.